ACS APPLIED NANO MATERIALS

www.acsanm.org

Forum Article

ZnO−Co_3O_4 Nanofibers/MXene Composite with Peroxidase-Like Activity for Ascorbic Acid Detection

Murilo H. M. Facure, Luiza A. Mercante, Yury Gogotsi,* and Daniel S. Correa*

Cite This: *ACS Appl. Nano Mater.* 2025, 8, 4291−4299

Read Online

ABSTRACT: The growing concern about nutrient-rich diets and health monitoring has motivated the search for simple, fast, and effective methods for detecting important nutrients in foodstuffs. In this scenario, colorimetric detection using nanostructures presenting enzymatic properties (nanozymes) has gained prominence due to its experimental simplicity and low cost. In this work, zinc oxide−cobalt oxide electrospun nanofibers (ZnO−Co_3O_4 NFs) were combined with titanium carbide ($Ti_3C_2T_x$) MXene for the colorimetric detection of ascorbic acid. The nanocomposite (ZnO−Co_3O_4 NFs/$Ti_3C_2T_x$) presented peroxidase-like activity with a high affinity for the chromogenic substrate 3,3,5,5-tetramethylbenzidine and fast reaction kinetics. Taking advantage of the catalytic properties of the developed nanocomposite, ascorbic acid was detected with high sensitivity (the limit of detection was 0.58 μmol L^{-1}) and selectivity, even in the presence of common interferents. The colorimetric sensor even detected ascorbic acid in orange juice, revealing its potential to be used as a reliable and sensitive portable method for food analysis.

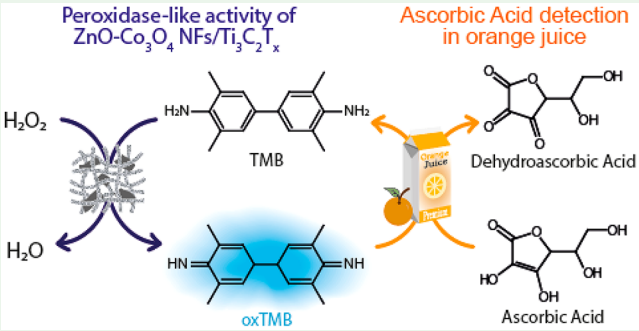

KEYWORDS: *nanozyme, colorimetric sensor, food analysis, peroxidase-mimetic activity, titanium carbide, MXene, electrospun nanofibers*

1. INTRODUCTION

Ascorbic acid (AA or Vitamin C) is a nutrient that has antioxidant properties and plays a pivotal role in human physiological and biochemical processes. Like other vitamins, AA must be regularly ingested in small and precise quantities for the body's normal function. Its deficiency has been associated with the development of health issues such as scurvy[1] and mental illness.[2] In addition, AA exhibits a correlation between the synthesis of collagen fibers and the assimilation of iron by the human body.[3,4] Humans ingest Vitamin C mainly by consuming foods rich in this nutrient, especially citrus fruits or their derived foods.[5] In this scenario, to ensure precise control over the concentration of AA in food samples, producers necessitate expeditious and straightforward methods for the rapid detection and quantification of AA.[3,5]

Many techniques have been reported for the detection of AA, including voltammetry techniques,[6−8] high-performance liquid chromatography,[9,10] electrophoresis,[11,12] and chemiluminescence.[13,14] Despite presenting high accuracy and sensitivity, such methods usually demand sophisticated equipment and highly trained personnel. In this scenario, the colorimetric detection of AA may represent a simpler, faster, and low-cost alternative.[15,16] Due to their high catalytic efficiency, stability, and low cost, nanozymes, i.e., nanostructures with enzyme-like activities, have been successfully employed to design colorimetric sensors.[4,17,18] The detection is usually performed by catalyzing the oxidation of a chromogenic substrate, e.g., 3,3,5,5-tetramethylbenzidine (TMB), with the nanozyme and, subsequently, reducing the oxidized substrate by adding the analyte to the reaction medium. The color changes can be monitored, for instance, by absorbance variations, and the concentration of the analyte can then be determined.[19,20]

The catalytic performance of nanozymes is inherently influenced by their constituent materials. Among the diverse range of nanomaterials with reported catalytic activities akin to natural enzymes, such as oxidases[21] and peroxidases,[22,23] carbon-based materials[24,25] and metal oxide[26,27] and metal nanostructures[28,29] have demonstrated excellent catalytic activity.[30−32] On the other hand, the utilization of MXenes as nanozymes remains underexplored, with a limited number of studies reporting their potential.[30,33] MXenes are a new family of 2D transition metal carbides, nitrides, and carbonitrides with large active surface area,[34] high conductivity,[35] and acceptable biocompatibility[36] and can be easily dispersed in water,[37] making them promising materials to compose nanostructures with enzyme-like activities.[38−40]

Special Issue: Forum Focused on South American Authors

Received: January 25, 2024
Revised: March 29, 2024
Accepted: April 4, 2024
Published: April 13, 2024

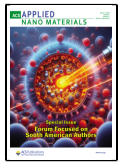

https://doi.org/10.1021/acsanm.4c00539
ACS Appl. Nano Mater. 2025, 8, 4291−4299

Furthermore, combining MXene with other nanostructures can give rise to synergic effects, which have not yet been fully explored.

Herein, we developed a novel MXene-based nanozyme with superior catalytic properties. Specifically, we synergistically combined zinc oxide−cobalt oxide electrospun nanofibers (Scheme 1a(i)) with $Ti_3C_2T_x$ MXene (Scheme 1a(ii)), which yielded a nanozyme (ZnO−Co_3O_4 NFs/$Ti_3C_2T_x$) with a high peroxidase-like catalytic performance, presenting remarkable kinetic parameters. This is the first time $Ti_3C_2T_x$ MXene has been combined with inorganic nanofibers to be used as nanozymes. The enhanced performance can be attributed to the composition of the materials since metal oxides have demonstrated excellent catalytic properties, while MXenes possess exposed active sites displaying peroxidase-like activity.[30,41] Moreover, the 1D and 2D structures of the constituent materials give rise to a nanocomposite with a large specific surface area. The composite displayed high sensitivity for the colorimetric detection of AA in actual juice samples, as illustrated in Scheme 1b.

Scheme 1. (a) Schematic Illustration of the (i) ZnO−Co_3O_4 NFs and (ii) $Ti_3C_2T_x$ Syntheses; (b) Peroxidase-Like Activity of the ZnO−Co_3O_4 NFs/$Ti_3C_2T_x$ Nanozyme and Colorimetric Detection of Ascorbic Acid

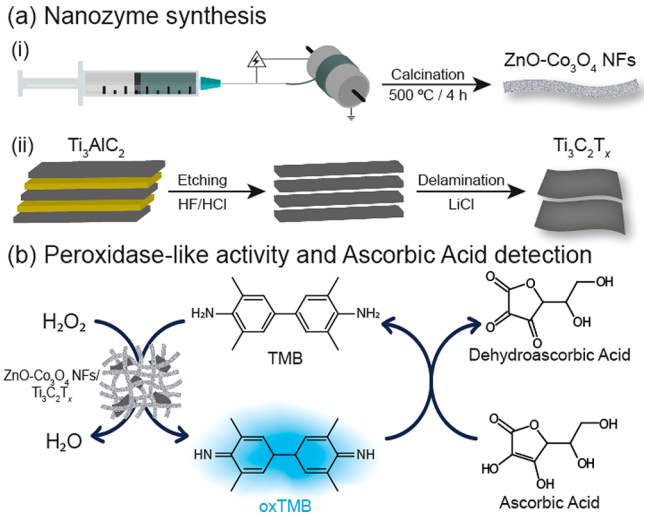

2. EXPERIMENTAL SECTION

2.1. Materials. Zinc nitrate ($Zn(NO_3)_2{\cdot}6H_2O$), poly(vinylpyrrolidone) (PVP, Mw 1,300,000), and *N,N*-dimethylformamide (DMF), purchased from Sigma-Aldrich, and cobalt acetate ($Co(CH_3COO)_2{\cdot}6H_2O$), supplied by Synth, Brazil, were used in the electrospun nanofiber production. TiC (99.5%, 2 μm powder), Ti (99.5%, 325 mesh), and Al (99.5%, 325 mesh) used in the MAX phase synthesis were purchased from Alfa Aesar. Hydrofluoric acid (HF, 40%, Vetec), hydrochloric acid (HCl, 36%, Synth), and lithium chloride (LiCl, Synth) were used in the MXene etching and delamination.

Acetic acid (CH_3COOH) and sodium acetate (CH_3COONa) were purchased from Synth and used in the preparation of the acetate buffer (0.1 mol L^{-1}, pH 4). 3,5,3′,5′-Tetramethylbenzidine (TMB) and L-ascorbic acid (AA, ≥99%) were obtained from Sigma-Aldrich. Hydrogen peroxide (H_2O_2, 35%) was purchased from Neon, Brazil. Sodium citrate (Synth), citric acid (Synth), potassium chloride (KCl, ≥99%, Synth), sodium chloride (NaCl, ≥99%, Synth), D-(+)-glucose (≥99%, Vetec), sucrose (Hexis), and sorbitol (D-sorbitol, 99%, Vetec) were used in the interferent tests.

The orange juices used in the sample analysis were purchased from a local market.

2.2. ZnO−Co_3O_4 NFs/$Ti_3C_2T_x$ Synthesis. The Ti_3AlC_2 MAX phase used in the MXene synthesis was prepared as described elsewhere.[42] $Ti_3C_2T_x$ synthesis was performed by etching the Al layer of the MAX phase, adapted from a previously reported method.[43] In the synthesis, a mixture containing 2 g of the MAX phase, 11.2 mL of DI water, 24 mL of HCl (11.65 mol L^{-1}), and 4.8 mL of HF (22.6 mol L^{-1}) was stirred at 35 °C for 24 h. The multilayer MXene was obtained by successive centrifugation steps (3500 rpm for 5 min) until the pH of the supernatant was higher than 6. Then, the obtained slurry was dispersed in 100 mL of a 0.5 M LiCl solution and stirred for 24 h at room temperature. The LiCl was removed by centrifugation (3500 rpm for 5 min), and the delaminated $Ti_3C_2T_x$ was collected when the supernatant started to become a black color.

To produce the ZnO−Co_3O_4 electrospun NFs, 0.5 g of PVP, 0.4 g of $Zn(NO_3)_2{\cdot}6H_2O$, and 0.2 g of $Co(CH_3COO)_2{\cdot}6H_2O$ were dissolved in 5 mL of DMF under stirring for 6 h at room temperature. The nanofibers were prepared by electrospinning on an electric field of 20 kV, a working distance of 6 cm, and a feed rate of 0.3 mL h^{-1}. Subsequently, ZnO−Co_3O_4 nanofibers were synthesized by calcinating the precursor fibers at 500 °C for 4 h in a muffle furnace with a heating rate of 10 °C min^{-1}.

The ZnO−Co_3O_4 NFs/$Ti_3C_2T_x$ composite was obtained by adding 60 mg of the nanofibers and 0.8 mL of a 1 mg/mL $Ti_3C_2T_x$ dispersion to 3.2 mL of water. Then, bath sonication (5 min) was used to ensure the dispersion of the materials.

2.3. Physicochemical Characterization. A Scanning Electron Microscope (SEM, FEI Magellan 400 L, USA) was used to evaluate the morphology of the materials, which were deposited onto a silicon substrate by drop-casting. Energy Dispersive X-ray Spectroscopy (EDS) was performed using a SEM instrument (JEOL, JSM 6510, Japan). The nanocomposite was deposited on a silicon substrate. X-ray diffraction (XRD) measurements were carried out in a Shimadzu XRD-6000 diffractometer (Japan) using the MAX phase powder and the vacuum-filtrated $Ti_3C_2T_x$ films. The experimental parameters were Cu K_α radiation (λ = 0.154059 nm), 30 kV, and 30 mA (Shimadzu XRD-6000). X-ray photoelectron spectroscopy (XPS) measurements were performed with the material's powder on an ESCALAB-MKII spectrometer (excitation source of 1486.6 eV). Fourier transform infrared (FTIR) spectroscopy was carried out on a Bruker Vertex 70 spectrometer (USA). 64 scans were collected from 4000 to 400 cm^{-1} using the attenuated total reflectance (ATR) mode and the materials' powder.

2.4. Peroxidase-Like Activity of ZnO−Co_3O_4 NFs/$Ti_3C_2T_x$. To evaluate the peroxidase-like activity of the nanomaterials, UV−vis time-dependent kinetic studies were performed to monitor changes in the solution color associated with oxidation of the TMB chromogenic substrate. The kinetic constants were calculated using the Michaelis−Menten equation[44,45]

$$\nu = \frac{\nu_{max}[S]}{K_m + [S]} \quad (1)$$

where ν_i and ν_{max} are the initial and maximum reaction velocities, K_m is the Michaelis−Menten constant, which is associated with the affinity of the nanozyme for the substrate, and [*S*] represents the substrate concentration.[30] The tests were carried out in acetate buffer solution, which was used to correct the final volume to 2 mL. To evaluate the affinity with TMB, 15 μL of the nanozyme dispersion (15 mg mL^{-1}) and 200 μL of H_2O_2 (1 mol L^{-1}) were added to the buffer solution, and the TMB concentration was varied from 0.05 to 0.7 mmol L^{-1}. To estimate the affinity with H_2O_2, 15 μL of the nanozyme solution (15 mg mL^{-1}) and 10 μL of TMB (5 mg mL^{-1}) were used, and the H_2O_2 concentration varied from 0.05 to 1.0 mol L^{-1}. UV−vis spectra were collected from 320 to 750 nm, and the absorbance at 652 nm, the wavelength used to monitor the TMB chromogenic reaction, was recorded with 45 s time intervals.[45,46]

https://doi.org/10.1021/acsanm.4c00539
ACS Appl. Nano Mater. 2025, 8, 4291−4299

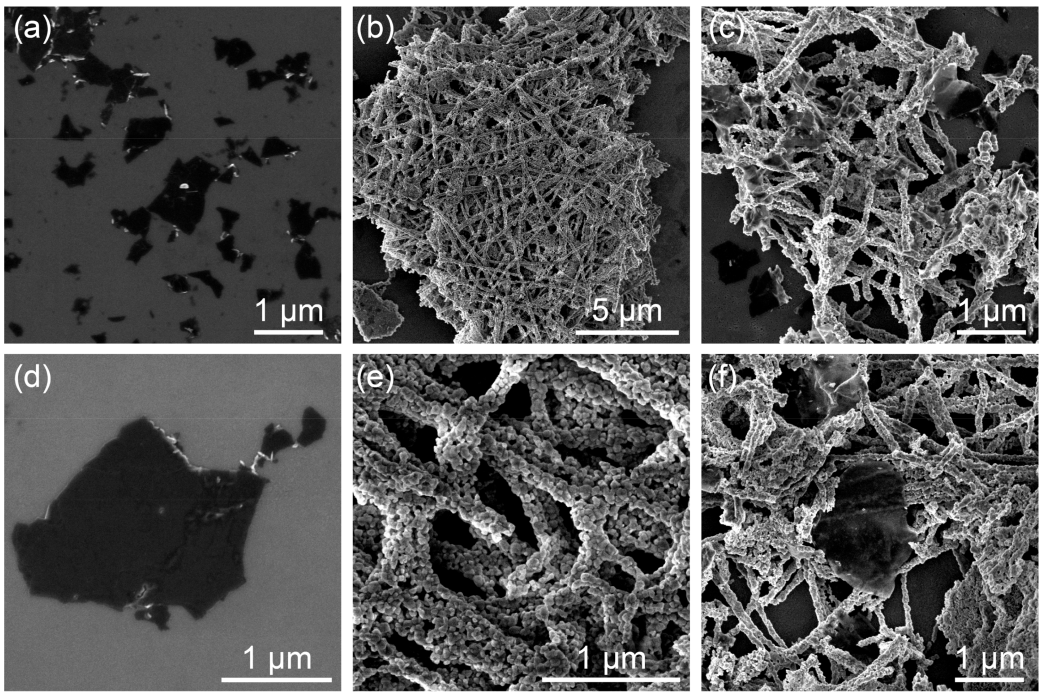

Figure 1. SEM images of (a and d) $Ti_3C_2T_x$ MXene flakes, (b and e) ZnO−Co_3O_4 NFs, and (c and f) ZnO−Co_3O_4 NFs/$Ti_3C_2T_x$ nanocomposite.

To calculate the kinetic parameters (ν_{max} and K_m), the collected data were fitted by the Lineweaver−Burk plot:[46]

$$\frac{1}{\nu} = \frac{K_m}{\nu_{max}}\left(\frac{1}{[S]} + \frac{1}{K_m}\right) \quad (2)$$

The Beer−Lambert Law was used to convert the absorbance data to the concentration $[S]$.

2.5. Colorimetric Detection of Ascorbic Acid. The detection of AA was carried out by monitoring the fading of the blue oxidized TMB (oxTMB) solution after AA addition. In the process, 15 μL of the nanozyme dispersion was added to an acetate buffer solution containing 0.4 mol L^{-1} of H_2O_2 and 0.1 mmol L^{-1} of TMB. The solution was incubated for 15 min, and then the absorbance of the blank (A_0) at 652 nm was recorded. Next, a certain concentration of AA was added to the solution, and the absorbance was again recorded at 652 nm after 1 min (A_1). A concentrated AA solution (0.1 mol L^{-1}) was used to avoid dilution effects. A calibrated curve was obtained using the concentration of the AA added and the difference in the absorbance recorded before and after AA addition ($\Delta Abs = A_0 - A_1$). The limit of detection (LOD) was calculated using the $3\sigma/S$ ratio, in which σ is the standard deviation of the lowest concentration of AA added and S is the slope of the calibration curve.[18] The interferent tests were performed using the same procedure but using a fixed concentration of interferents (500 mmol L^{-1}).

2.6. Real Sample Analysis. The feasibility of AA detection by the ZnO−Co_3O_4 NFs/$Ti_3C_2T_x$ nanozyme was evaluated by using commercial orange juices: fresh orange juice, carton orange juice, and orange juice powder. The orange juice from the powder was prepared according to the instructions on the packaging. Before use, juice samples were filtered using a 0.22 μm pore size membrane (Macherey-Nagel) and diluted 50 times with the acetate buffer solution. The same procedure described in the last section was used with spiked and nonspiked samples. The recovery of AA was calculated using the calibration curve obtained previously.

3. RESULTS AND DISCUSSION

3.1. Materials Characterization. XRD characterization was carried out to confirm the $Ti_3C_2T_x$ MXene synthesis and formation of the ZnO−Co_3O_4 NFs. Figure S1a shows the XRD pattern of the Ti_3AlC_2 MAX phase and the $Ti_3C_2T_x$ film. While the Ti_3AlC_2 pattern presents all the crystallographic peaks, the MXene shows only the (00l) peaks, confirming the etching and delamination of the MAX phase.[47] Also, the (002) peak shifted from 9.5° to 7.7°, indicating a higher interlayer spacing of MXene, contributing to a greater available surface area. The XRD pattern obtained for the ZnO−Co_3O_4 NFs (Figure S1b) shows typical diffraction peaks of the ZnO wurtzite structure (JCPDS nº 36-1451) and Co_3O_4 cubic phase (JCPDS nº 42-1467), confirming the crystalline structure obtained after the annealing.[48,49] No additional peaks were observed, which indicated the absence of impurities.

The morphologies of the MXene, the nanofibers, and the nanocomposite were evaluated by SEM (Figure 1) and TEM (Figure S2). As shown in Figure 1a,d and Figure S2a, isolated $Ti_3C_2T_x$ flakes were obtained after etching and delamination. The flakes presented defined edges with no apparent defects, indicating a high-quality MXene.[50] The ZnO−Co_3O_4 NFs, shown in Figure 1b, presented a mean diameter of 129 ± 24 nm (n = 50 measures). In Figure 1e, one can see more clearly the wrinkled surface of the obtained nanofibers due to the formation of ZnO and Co_3O_4 nanoparticles. The TEM image of a ZnO−Co_3O_4 NF (Figure S2b) reveals the crystalline structure of the metal oxides wrapped in a thin layer of carbon. The interaction of the MXene with the nanofibers can be visualized in Figure 1c and f, in which it is possible to observe nanofibers located either onto the MXene layers (Figures 1c) or involving them (Figure 1f).

EDS analysis was employed to investigate the composition of the nanocomposite. As shown in Figure S3, besides the C and O elements present in both materials, the images revealed the presence of Co and Zn from the ZnO−Co_3O_4 NFs and Ti from the MXene. The images also show that the constituent materials of the nanozyme are evenly distributed, indicating that the nanocomposite was successfully synthesized.

The nanocomposite was also characterized by FTIR and XPS (Figure S4). The $Ti_3C_2T_x$ FTIR spectrum presents bands

https://doi.org/10.1021/acsanm.4c00539
ACS Appl. Nano Mater. 2025, 8, 4291−4299

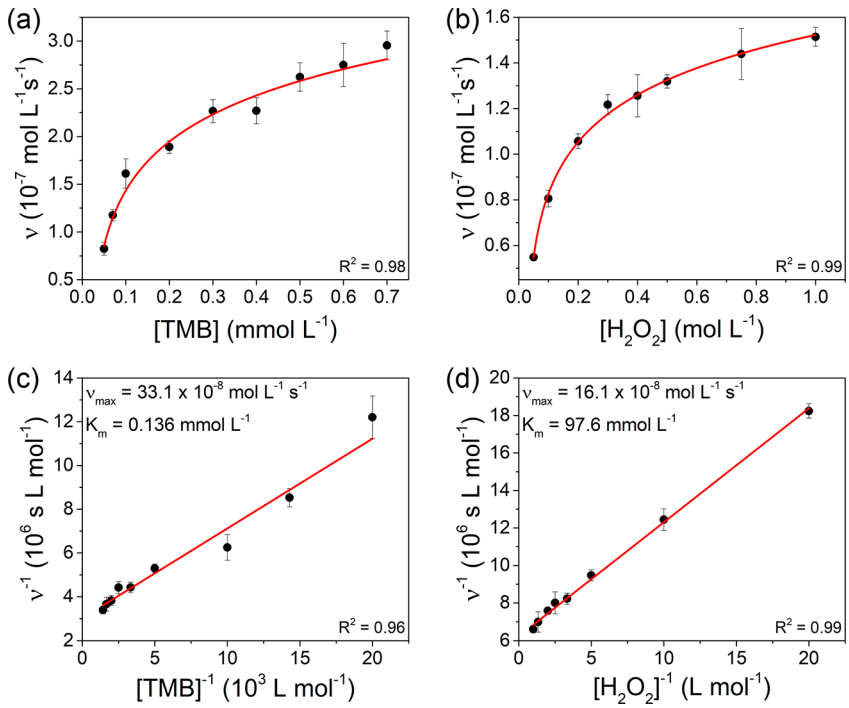

Figure 2. Catalytic kinetics of the ZnO−Co_3O_4 NFs/$Ti_3C_2T_x$ nanozyme as peroxidase mimicking. Michaelis−Menten curves for different amounts of (a) TMB and (b) H_2O_2 and Lineweaver−Burk plots for (c) TMB and (d) H_2O_2 with the respective values of ν_{max} and K_m parameters.

related to hydroxyl groups at 1651 cm^{-1} and between 3200 and 3600 cm^{-1}, which can be ascribed to adsorbed water on the MXene surface. The peaks at 2927 and 2852 cm^{-1} are related to symmetric and asymmetric stretching vibrations of C—H bonds, while the peak at 1090 cm^{-1}, attributed to the stretching vibration of the C—F bond, indicates a functionalization of the MXene surface during etching.[51,52] The deformation vibration of the Ti—O and Ti—C bonds can be ascribed to the bands at 634 and 573 cm^{-1}, respectively.[52,53] The ZnO—Co_3O_4 NF spectrum presented bands centered at 2348, 1578, and 1410 cm^{-1} attributed to the C≡N, C═O, and C═C bonds, respectively, due to the presence of residual surface carbon in the nanofibers.[54,55] The bands between 535 and 760 cm^{-1} can be ascribed to the Zn—O and Co—O vibrations.[56−58] The nanocomposite spectrum presents the same bands of the constituent materials and does not present any additional peak. Minor shifts of the C═O and C═C bands can be ascribed to the interaction between the materials by van der Waals forces, indicating the success in obtaining the nanocomposite.[59]

The XPS $Ti_3C_2T_x$ survey spectrum shows peaks related to Ti, C, O, F, and Cl elements (Figure S4b). While Ti and C are from the structure of the MXene, O, F, and Cl can be present as surface terminations.[47] The MXene Ti 2p high-resolution spectra (Figure S5a) also show peaks related to the Ti−C bonds and from adsorbed oxygen onto the MXene surface.[60,61] The survey spectrum of the nanofibers (Figure S4b) shows a C 1s peak related to the residual surface carbon structure, Zn, Co, and O peaks from the metal oxide phases. The ZnO−Co_3O_4 NFs/$Ti_3C_2T_x$ nanozyme spectrum presented only the peaks associated with the ZnO−Co_3O_4 NFs, probably due to the smaller amount of MXene in the nanocomposite. The high-resolution Zn 2p and Co 2p spectra are presented in Figure S5b and c. The Zn 2p spectrum has two sharp peaks centered at 1045 and 1022 eV related to the Zn $2p_{1/2}$ and Zn $2p_{3/2}$, respectively, indicating the presence of Zn^{2+}. The energy difference between the two peaks was found to be 23.1 eV, in accordance with other works.[62,63] The Co 2p spectrum could be deconvoluted in peaks related to Co^{3+}, Co^{2+}, and their satellite peaks, indicating that Co is present in two different oxidation states at the NF surface.[64] The Zn 2p and Co 2p spectra of the nanocomposite (Figure S5d and e) did not show remarkable changes after combining the MXene with the NFs, indicating their stability.

3.2. Peroxidase-Like Catalytic Activity. The peroxidase-mimetic ability of the ZnO−Co_3O_4 NFs/$Ti_3C_2T_x$ nanozyme was evaluated by monitoring the conversion of the TMB substrate in its oxidized form, which presents a blue color. Besides the nanocomposite, the isolated materials were also tested. As shown in Figure S6a, ZnO−Co_3O_4 NFs and $Ti_3C_2T_x$ presented some peroxidase-like activity. These properties can be mainly ascribed to the different valence states of the metal atoms of the nanofibers and the exposed active sites of the $Ti_3C_2T_x$ MXene.[30,41] However, the constituent materials alone gave an inferior performance compared to that of the hybrid material. Notice that the performance of the ZnO−Co_3O_4 NFs/$Ti_3C_2T_x$ nanozyme is greater than the sum of the performances of the isolated materials (ca. 85% of the ZnO−Co_3O_4 NFs/$Ti_3C_2T_x$ performance). This suggests that a synergistic effect is obtained by combining the nanofibers with MXene, giving rise to a nanocomposite with superior catalytic activity. The synergistic effect is probably due to the novel architecture formed when combining the nanomaterials. The van der Waals forces between the ZnO−Co_3O_4 NFs and the MXene can lead to more suitable conformations, giving rise to a nanocomposite with a higher specific surface area and a superior performance.[18,65]

Different ratios of ZnO−Co_3O_4 NFs and $Ti_3C_2T_x$ were tested in preliminary experiments (results not shown). The ratio used in this investigation was found to present higher

https://doi.org/10.1021/acsanm.4c00539
ACS Appl. Nano Mater. 2025, 8, 4291−4299

catalytic activity. As shown in Figure S6a, MXene presents an inferior peroxidase-like performance; therefore, ratios containing higher amounts of MXene led to a decrease in the nanocomposite activity. Since there is a synergistic effect by combining the materials, the optimum amount of MXene was used to take advantage of the synergistic effect without compromising the nanozyme performance.

The performance of the ZnO−Co_3O_4 NFs/$Ti_3C_2T_x$ nanozyme was also evaluated at different pH values. As observed for other nanozymes,[4,66,67] the peroxidase-like activity is higher at pH 4 (Figure S6b). The higher activity at acidic pH values can be mainly ascribed to a buffer coating formation over the nanozyme surface. At this pH, the TMB is partially positively charged and remains attached to the outer coating of the nanozyme. In contrast, the H_2O_2 passes through the buffer coating, reaching the nanozyme surface, decomposing into ·OH radicals that oxidize TMB.[68] Based on these results, all of the hereafter experiments were carried out using buffer acetate with pH 4.

The Michaelis−Menten model was used to estimate the performance of the nanozyme by calculating the ν_{max} and K_m kinetic parameters (eq 1).[45,46] Figure S7 (a) and (b) shows the TMB and H_2O_2 reaction evolution catalyzed by the ZnO−Co_3O_4 NFs/$Ti_3C_2T_x$ nanozyme, respectively. The curves were used to calculate the initial reaction velocity (ν_i) of the Michaelis−Menten model. The Michaelis−Menten curves and the Lineweaver−Burk (eq 2) plots obtained are shown in Figure 2a,b and c,d, respectively.

Figure 3 shows a comparison between the peroxidase-like performance toward TMB oxidation of the ZnO−Co_3O_4 NFs/$Ti_3C_2T_x$ nanozyme and other reported materials as well as the natural horseradish peroxidase (HRP) enzyme. K_m is used to estimate the affinity of the nanozyme for the substrate—lower values indicate higher affinity.[30,31] Therefore, the further to the left in the graph, the greater the interaction of the nanozyme with the TMB substrate. The ZnO−Co_3O_4 NFs/$Ti_3C_2T_x$ nanozyme presented a K_m value of 0.136 mmol L^{-1} for TMB, indicating an affinity for the substrate higher than those of most similar nanozymes recently reported. Also, ZnO−Co_3O_4 NFs/$Ti_3C_2T_x$ presented fast kinetics with a ν_{max} value of 33.1 × 10^{-8} mol L^{-1} s^{-1}, indicating high reactivity of the nanozyme toward TMB oxidation. Moreover, the obtained kinetic parameters for the ZnO−Co_3O_4 NFs/$Ti_3C_2T_x$ nanozyme are superior to those of natural HRP. The ν_{max} and K_m values are presented in Table S1, as well as the values for H_2O_2 as a substrate.

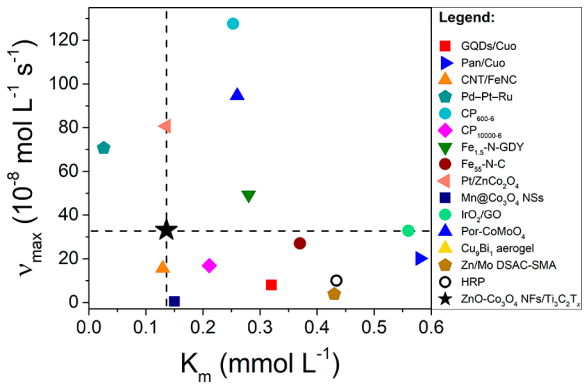

Figure 3. Comparison of the catalytic kinetic parameters (K_m and ν_{max}) of the ZnO−Co_3O_4 NFs/$Ti_3C_2T_x$ with other peroxidase-like nanozymes and the natural HRP for TMB. GQDs/CuO,[69] Pan/CuO,[4] CNT/FeNC,[70] Pd−Pt−Ru,[66] CP_{600-6},[67] $CP_{10000-6}$,[67] $Fe_{1,5}$−N−GDY,[71] Fe_{55}−N−C,[72] Pt/$ZnCo_2O_4$,[73] Mn@Co_3O_4 NSs,[74] IrO_2/GO,[3] Por−$CoMoO_4$,[75] Cu_9Bi_1 aerogel,[76] Zn/Mo DSAC−SMA,[77] HRP.[78]

3.3. Ascorbic Acid Detection. Given the good peroxidase mimicking performance obtained, the nanozyme was then used to detect AA. The detection is possible due to the chromogenic reaction of the TMB substrate and the peroxidase-like activity presented by the ZnO−Co_3O_4 NFs/$Ti_3C_2T_x$ nanocomposite. In the presence of the nanozyme and H_2O_2, the substrate is oxidized to oxTMB, which gives a blue color (Figure S8a). Upon addition of AA, the analyte reacts with oxTMB, producing TMB, causing color fading and dehydroascorbic acid, as illustrated in Scheme 1b. Since this color change is proportional to the amount of AA added, its detection can be performed by monitoring the absorbance value change at 652 nm.

Figure 4a shows a linear relationship between the amount of AA added and the ΔAbs recorded at 652 nm. The calculated LOD ($3\sigma/S$) was found to be 0.58 μmol L^{-1}. The comparison of ZnO−Co_3O_4 NFs/$Ti_3C_2T_x$ composite sensitivity toward AA detection with other nanozymes is presented in Table 1. Since different nanozyme compositions give rise to particular kinetics, i.e., unique values of K_m and ν_{max}, the performance is expected to vary according to the nanozyme used. The LOD obtained in this work is comparable or even superior to recently reported values achieved using similar peroxidase-like nanozymes. Moreover, unlike other techniques used to detect AA, such as electrochemical,[79,80] high-performance liquid chromatography,[81] and electrochemiluminescence,[82] the colorimetric method reported here does not require sophisticated equipment, besides being simpler and faster.

Aiming to employ the material to detect AA in actual food samples, possible interferent tests were performed using substances commonly found in juice, including sodium citrate, citric acid, KCl, NaCl, glucose, sucrose, and sorbitol. As can be seen in Figure 4b, the addition of interferents at 500 μmol L^{-1} did not show significant changes in the absorbance values at 652 nm, while the addition of 100 μmol L^{-1} of AA led to a total fading of the blue color solution. Such behavior can be visualized in Figure S8b,c, in which digital pictures of the TMB solution are displayed immediately after and 1 min after adding the AA and the interferents.

3.4. Real Sample Analyses. Tests with interfering agents demonstrated the potential of the as-developed nanozyme system for AA detection in food samples. For this, orange juice, known to have a significant AA content, was chosen as a sample. Three commercial juices were tested: fresh orange juice, carton orange juice, and orange juice from powder. Table 2 shows the amount of AA found in each orange juice sample and the recovery obtained after the addition of the analyte. The measurements were performed in triplicate. All the recovery values were close to 100%, indicating the capacity of the sensor to estimate the amount of AA in actual food samples within varied concentrations in an easy, low-cost, and expedited way.

4. CONCLUSIONS

Herein, ceramic electrospun nanofibers (ZnO−Co_3O_4 NFs) were combined with $Ti_3C_2T_x$ MXene to obtain a material with peroxidase-like catalytic activity. The nanocomposite was thoroughly characterized, and its performance as a nanozyme

https://doi.org/10.1021/acsanm.4c00539
ACS Appl. Nano Mater. 2025, 8, 4291−4299

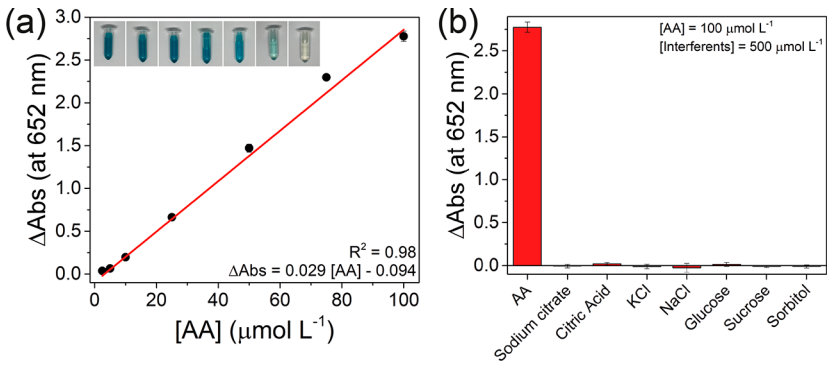

Figure 4. (a) Linear regression curve of AA detection using the ZnO−Co_3O_4 NFs/$Ti_3C_2T_x$ nanozyme. The inset pictures show the color change with the addition of different amounts of AA (from 2.5 to 100 μmol L^{-1}). (b) Comparison of the colorimetric responses for AA and interferents.

Table 1. Comparative Performance of ZnO−Co_3O_4 NFs/$Ti_3C_2T_x$ with Other Peroxidase-Like Nanozymes for AA Detection in Acetate Buffer

Nanozyme	Linear Range (μmol L^{-1})	LOD (μmol L^{-1})	Ref.
Pan/Cuo	1−180	0.56	4
CNT/FeNC	0.1−10	0.03	70
Pd−Pt−Ru	2−12	1.13	66
d-CoFe-LDHs	20−625	3.6	83
CP_{600-6}	0.8−80	35	67
Mn@Co_3O_4	1−8	0.4	74
Pt/$ZnCo_2O_4$	1−15	0.456	73
IrO_2/GO	5−70	0.324	3
Fe−CuO	5−50	4.66	84
Fe_3O_4/CoFe-LDH	0.5−10	0.2	85
Cu_9Bi_1 aerogel	0.3−0.9	0.059	76
Pd−Pt−Ir	25−800	11.7	86
ZnO−Co_3O_4 NFs/$Ti_3C_2T_x$	2.5−100	0.58	This work

was evaluated, showing a synergic effect of ZnO−Co_3O_4 NFs and the $Ti_3C_2T_x$. The kinetic parameters revealed a high affinity of the nanozyme toward the TMB substrate (K_m of 0.136 mmol L^{-1}) and a fast reaction rate (ν_{max} = 33.1 × 10^{-8} mol L^{-1} s^{-1}). The composite material was used to detect ascorbic acid by changing the oxidation state of the chromogenic TMB substrate. A low limit of detection of 0.58 μmol L^{-1} was obtained, and tests in real orange juice samples demonstrated the potential of the ZnO−Co_3O_4 NFs/$Ti_3C_2T_x$ nanozyme to be used in the detection of ascorbic acid in juice simply and reliably with high accuracy. The results pave the way for future detection and monitoring of ascorbic acid concentrations in food and other environments, such as in body fluids.

■ ASSOCIATED CONTENT

Supporting Information

The Supporting Information is available free of charge at https://pubs.acs.org/doi/10.1021/acsanm.4c00539.

XRD patterns of the Ti_3AlC_2 MAX phase, $Ti_3C_2T_x$ MXene, and ZnO-Co_3O_4 NFs, TEM images of $Ti_3C_2T_x$ and ZnO-Co_3O_4 NFs, EDS images of the ZnO-Co_3O_4 NFs/$Ti_3C_2T_x$ nanozyme, FTIR and XPS spectra of $Ti_3C_2T_x$, ZnO-Co_3O_4 NFs, and ZnO-Co_3O_4 NFs/$Ti_3C_2T_x$, high-resolution XPS spectra of Ti 2p, Zn 2p, and Co 2p, comparison of the catalytic performance of the nanozyme and the isolated materials, performance of the nanozyme in different pH values, reaction−time curves of the TMB colorimetric reaction, comparison of the kinetic parameters obtained for ZnO−Co_3O_4 NFs/$Ti_3C_2T_x$ with other reported nanozymes, and TMB solution color change after the addition of AA (PDF)

■ AUTHOR INFORMATION

Corresponding Authors

Yury Gogotsi − *A. J. Drexel Nanomaterials Institute and Department of Materials Science and Engineering, Drexel University, Philadelphia, Pennsylvania 19104, United States;* orcid.org/0000-0001-9423-4032; Email: gogotsi@drexel.edu

Daniel S. Correa − *Nanotechnology National Laboratory for Agriculture (LNNA), Embrapa Instrumentação, 13560-970 Sao Carlos, SP, Brazil; PPGQ, Department of Chemistry, Center for Exact Sciences and Technology, Federal University of Sao Carlos (UFSCar), 13565-905 Sao Carlos, SP, Brazil;* orcid.org/0000-0002-5592-0627; Email: daniel.correa@embrapa.br

Authors

Murilo H. M. Facure − *Nanotechnology National Laboratory for Agriculture (LNNA), Embrapa Instrumentação, 13560-970 Sao Carlos, SP, Brazil; PPGQ, Department of*

Table 2. Determination of AA in Orange Juice Samples Using the ZnO−Co_3O_4 NFs/$Ti_3C_2T_x$ Nanozyme

Fresh orange juice			Carton orange juice			Orange juice from powder		
Added (μmol L^{-1})	Found (μmol L^{-1})	Recovery (%)	Added (μmol L^{-1})	Found (μmol L^{-1})	Recovery (%)	Added (μmol L^{-1})	Found (μmol L^{-1})	Recovery (%)
0	9.3 ± 0.4		0	7.2 ± 0.1		0	2.8 ± 0.3	
24	32.5 ± 0.8	98.5 ± 2.4	24	29.9 ± 0.8	96.4 ± 2.6	24	26.8 ± 0.8	99.3 ± 2.9
64	73.3 ± 1.2	100.5 ± 1.7	64	70.6 ± 0.9	99.5 ± 1.3	64	66.1 ± 1.1	98.6 ± 1.7

https://doi.org/10.1021/acsanm.4c00539
ACS Appl. Nano Mater. 2025, 8, 4291−4299

Chemistry, Center for Exact Sciences and Technology, Federal University of Sao Carlos (UFSCar), 13565-905 Sao Carlos, SP, Brazil; A. J. Drexel Nanomaterials Institute and Department of Materials Science and Engineering, Drexel University, Philadelphia, Pennsylvania 19104, United States; orcid.org/0000-0003-0858-0364

Luiza A. Mercante − *Institute of Chemistry, Federal University of Bahia (UFBA), 40170-280 Salvador, BA, Brazil;* orcid.org/0000-0003-4206-6545

Complete contact information is available at: https://pubs.acs.org/10.1021/acsanm.4c00539

Funding

The Article Processing Charge for the publication of this research was funded by the Coordination for the Improvement of Higher Education Personnel - CAPES (ROR identifier: 00x0ma614).

Notes

The authors declare no competing financial interest.

■ ACKNOWLEDGMENTS

M.H.M.F. and D.S.C. thank FAPESP (2021/11683-8, 2017/10582-8, 2018/22214-6) and CNPq and MCTI-SisNano (CNPq/402.287/2013-4) from Brazil for the financial support. The authors also thank the Laboratory of Structural Characterization (LCE/DEMa/UFSCar) for the microscopy facilities and Dr. Valmor Mastelaro (IFSC-USP) for the XPS measurements.

■ REFERENCES

(1) Montalto, M.; Porceddu, E.; Pero, E.; Lupascu, A.; Gallo, A.; De Simone, C.; Nucera, E.; Aruanno, A.; Giarretta, I.; Pola, R.; Landolfi, R. Scurvy: A Disease Not to Be Forgotten. *Nutrition in Clinical Practice* **2021**, *36* (5), 1063−1067.

(2) Moretti, M.; Rodrigues, A. L. S.*Ascorbic Acid as an Antioxidant and Applications to the Central Nervous System*; Preedy, V. R., in Pathology: Oxidative Stress and Dietary Antioxidants, Ed.; Academic Press: 2020; Chapter 15, pp 159−167. DOI: 10.1016/B978-0-12-815972-9.00015-9.

(3) Sun, H.; Liu, X.; Wang, X.; Han, Q.; Qi, C.; Li, Y.; Wang, C.; Chen, Y.; Yang, R. Colorimetric Determination of Ascorbic Acid Using a Polyallylamine-Stabilized IrO_2/Graphene Oxide Nanozyme as a Peroxidase Mimic. *Microchimica Acta* **2020**, *187* (2), 110.

(4) Zheng, X.; Lian, Q.; Zhou, L.; Jiang, Y.; Gao, J. Peroxidase Mimicking of Binary Polyacrylonitrile-CuO Nanoflowers and the Application in Colorimetric Detection of H_2O_2 and Ascorbic Acid. *ACS Sustain Chem. Eng.* **2021**, *9* (20), 7030−7043.

(5) Porto, I. S. A.; Santos Neto, J. H.; dos Santos, L. O.; Gomes, A. A.; Ferreira, S. L. C. Determination of Ascorbic Acid in Natural Fruit Juices Using Digital Image Colorimetry. *Microchemical Journal* **2019**, *149*, No. 104031.

(6) Zhang, W.; Liu, L.; Li, Y.; Wang, D.; Ma, H.; Ren, H.; Shi, Y.; Han, Y.; Ye, B.-C. Electrochemical Sensing Platform Based on the Biomass-Derived Microporous Carbons for Simultaneous Determination of Ascorbic Acid, Dopamine, and Uric Acid. *Biosens Bioelectron* **2018**, *121*, 96−103.

(7) Wang, L.; Gong, C.; Shen, Y.; Ye, W.; Xu, M.; Song, Y. A Novel Ratiometric Electrochemical Biosensor for Sensitive Detection of Ascorbic Acid. *Sens Actuators B Chem.* **2017**, *242*, 625−631.

(8) Mazzara, F.; Patella, B.; Aiello, G.; O'Riordan, A.; Torino, C.; Vilasi, A.; Inguanta, R. Electrochemical Detection of Uric Acid and Ascorbic Acid Using R-GO/NPs Based Sensors. *Electrochim. Acta* **2021**, *388*, No. 138652.

(9) Szultka, M.; Buszewska-Forajta, M.; Kaliszan, R.; Buszewski, B. Determination of Ascorbic Acid and Its Degradation Products by High-Performance Liquid Chromatography-Triple Quadrupole Mass Spectrometry. *Electrophoresis* **2014**, *35* (4), 585−592.

(10) Szőcs, A.; Vancea, S.; Kiss, I.; Donáth-Nagy, G. Quantification of Plasma and Leukocyte Vitamin C by High Performance Liquid Chromatography with Mass Spectrometric Detection. *J. Anal. Chem.* **2020**, *75* (9), 1168−1176.

(11) Ribeiro, M. M. A. C.; Prado, A. A.; Domingues Batista, A.; Alejandro Abarza Munoz, R.; Mathias Richter, E. Rapid Method for Simultaneous Determination of Ascorbic Acid and Zinc in Effervescent Tablets by Capillary Zone Electrophoresis with Contactless Conductivity Detection. *J. Sep Sci.* **2019**, *42* (3), 754−759.

(12) Costa, B. M. C.; Prado, A. A.; Oliveira, T. C.; Bressan, L. P.; Munoz, R. A. A.; Batista, A. D.; da Silva, J. A. F.; Richter, E. M. Fast Methods for Simultaneous Determination of Arginine, Ascorbic Acid and Aspartic Acid by Capillary Electrophoresis. *Talanta* **2019**, *204*, 353−358.

(13) Wang, C.; Halawa, M. I.; Lou, B.; Gao, W.; Li, J.; Xu, G. Detection of Ascorbic Acid Based on Its Quenching Effect on Luminol−Artemisinin Chemiluminescence. *Analyst* **2021**, *146* (6), 1981−1985.

(14) Liu, P.; Meng, H.; Han, Q.; Zhang, G.; Wang, C.; Song, L.; Fu, Y. Determination of Ascorbic Acid Using Electrochemiluminescence Sensor Based on Nitrogen and Sulfur Doping Graphene Quantum Dots with Luminol as Internal Standard. *Microchimica Acta* **2021**, *188* (4), 120.

(15) Huang, L.; Sun, D. W.; Pu, H.; Wei, Q. Development of Nanozymes for Food Quality and Safety Detection: Principles and Recent Applications. *Compr Rev. Food Sci. Food Saf* **2019**, *18* (5), 1496−1513.

(16) Huang, Y.; Mu, X.; Wang, J.; Wang, Y.; Xie, J.; Ying, R.; Su, E. The Recent Development of Nanozymes for Food Quality and Safety Detection. *J. Mater. Chem. B* **2022**, *10* (9), 1359−1368.

(17) Navyatha, B.; Singh, S.; Nara, S. AuPeroxidase Nanozymes: Promises and Applications in Biosensing. *Biosens Bioelectron* **2021**, *175*, No. 112882.

(18) Facure, M. H. M.; Andre, R. S.; Cardoso, R. M.; Mercante, L. A.; Correa, D. S. Electrochemical and Optical Dual-Mode Detection of Phenolic Compounds Using MnO_2/GQD Nanozyme. *Electrochim. Acta* **2023**, *441*, No. 141777.

(19) Han, Y.; Luo, L.; Zhang, L.; Kang, Y.; Sun, H.; Dan, J.; Sun, J.; Zhang, W.; Yue, T.; Wang, J. Oxidase-like Fe−Mn Bimetallic Nanozymes for Colorimetric Detection of Ascorbic Acid in Kiwi Fruit. *Lwt* **2022**, *154*, No. 112821.

(20) Liu, X.; Yang, J.; Cheng, J.; Xu, Y.; Chen, W.; Li, Y. Facile Preparation of Four-in-One Nanozyme Catalytic Platform and the Application in Selective Detection of Catechol and Hydroquinone. *Sens Actuators B Chem.* **2021**, *337*, No. 129763.

(21) Chong, Y.; Liu, Q.; Ge, C. Advances in Oxidase-Mimicking Nanozymes: Classification, Activity Regulation and Biomedical Applications. *Nano Today* **2021**, *37*, No. 101076.

(22) Wang, H.; Wan, K.; Shi, X. Recent Advances in Nanozyme Research. *Adv. Mater.* **2019**, *31* (45), No. 1805368.

(23) Attar, F.; Shahpar, M. G.; Rasti, B.; Sharifi, M.; Saboury, A. A.; Rezayat, S. M.; Falahati, M. Nanozymes with Intrinsic Peroxidase-like Activities. *J. Mol. Liq.* **2019**, *278*, 130−144.

(24) Nirala, N. R.; Abraham, S.; Kumar, V.; Bansal, A.; Srivastava, A.; Saxena, P. S. Colorimetric Detection of Cholesterol Based on Highly Efficient Peroxidase Mimetic Activity of Graphene Quantum Dots. *Sens Actuators B Chem.* **2015**, *218*, 42−50.

(25) Wang, X.; Qu, K.; Xu, B.; Ren, J.; Qu, X. Multicolor Luminescent Carbon Nanoparticles: Synthesis, Supramolecular Assembly with Porphyrin, Intrinsic Peroxidase-like Catalytic Activity and Applications. *Nano Res.* **2011**, *4* (9), 908−920.

(26) Zhu, M.; Dai, Y.; Wu, Y.; Liu, K.; Qi, X.; Sun, Y. Bandgap Control of α -Fe_2O_3 Nanozymes and Their Superior Visible Light Promoted Peroxidase-like Catalytic Activity. *Nanotechnology* **2018**, *29* (46), No. 465704.

(27) Liu, X.; Yan, L.; Ren, H.; Cai, Y.; Liu, C.; Zeng, L.; Gao, J.; Liu, A. Facile Synthesis of Magnetic Hierarchical Flower-like Co_3O_4 Spheres: Mechanism, Excellent Tetra-Enzyme Mimics and Their Colorimetric Biosensing Applications. *Biosens Bioelectron* **2020**, *165*, No. 112342.
(28) Liu, C.-P.; Chen, K.-C.; Su, C.-F.; Yu, P.-Y.; Lee, P.-W. Revealing the Active Site of Gold Nanoparticles for the Peroxidase-Like Activity: The Determination of Surface Accessibility. *Catalysts* **2019**, *9* (6), 517.
(29) Wei, J.; Chen, X.; Shi, S.; Mo, S.; Zheng, N. An Investigation of the Mimetic Enzyme Activity of Two-Dimensional Pd-Based Nanostructures. *Nanoscale* **2015**, *7* (45), 19018−19026.
(30) Ballesteros, C. A. S.; Mercante, L. A.; Alvarenga, A. D.; Facure, M. H. M.; Schneider, R.; Correa, D. S. Recent Trends in Nanozymes Design: From Materials and Structures to Environmental Applications. *Mater. Chem. Front* **2021**, *5* (20), 7419−7451.
(31) Wei, H.; Wang, E. Nanomaterials with Enzyme-like Characteristics (Nanozymes): Next-Generation Artificial Enzymes. *Chem. Soc. Rev.* **2013**, *42* (14), 6060−6093.
(32) Lin, Y.; Ren, J.; Qu, X. Catalytically Active Nanomaterials: A Promising Candidate for Artificial Enzymes. *Acc. Chem. Res.* **2014**, *47* (4), 1097−1105.
(33) Zhu, X.; Lin, L.; Wu, R.; Zhu, Y.; Sheng, Y.; Nie, P.; Liu, P.; Xu, L.; Wen, Y. Portable Wireless Intelligent Sensing of Ultra-Trace Phytoregulator α-Naphthalene Acetic Acid Using Self-Assembled Phosphorene/Ti_3C_2-MXene Nanohybrid with High Ambient Stability on Laser Induced Porous Graphene as Nanozyme Flexible Electrode. *Biosens Bioelectron* **2021**, *179*, No. 113062.
(34) Xie, K.; Wang, J.; Xu, S.; Hao, W.; Zhao, L.; Huang, L.; Wei, Z. Application of Two-Dimensional MXene Materials in Sensors. *Mater. Des* **2023**, *228*, No. 111867.
(35) Gogotsi, Y.; Huang, Q. MXenes: Two-Dimensional Building Blocks for Future Materials and Devices. *ACS Nano* **2021**, *15* (4), 5775−5780.
(36) Iravani, S.; Varma, R. S. MXenes and MXene-Based Materials for Tissue Engineering and Regenerative Medicine: Recent Advances. *Mater. Adv.* **2021**, *2* (9), 2906−2917.
(37) Gogotsi, Y.; Anasori, B. The Rise of MXenes. *ACS Nano* **2019**, *13* (8), 8491−8494.
(38) Iravani, S.; Varma, R. S. MXene-Based Composites as Nanozymes in Biomedicine: A Perspective. *Nanomicro Lett.* **2022**, *14* (1), 213.
(39) Gogotsi, Y. *MXenes: From Discovery to Applications of Two-Dimensional Metal Carbides and Nitrides*, 1st ed.; Jenny Stanford Publishing: 2023.
(40) VahidMohammadi, A.; Rosen, J.; Gogotsi, Y. The World of Two-Dimensional Carbides and Nitrides (MXenes). *Science* **2021**, *372* (6547), No. eabf1581.
(41) Li, M.; Peng, X.; Han, Y.; Fan, L.; Liu, Z.; Guo, Y. Ti_3C_2 MXenes with Intrinsic Peroxidase-like Activity for Label-Free and Colorimetric Sensing of Proteins. *Microchemical Journal* **2021**, *166* (March), No. 106238.
(42) Mathis, T. S.; Maleski, K.; Goad, A.; Sarycheva, A.; Anayee, M.; Foucher, A. C.; Hantanasirisakul, K.; Shuck, C. E.; Stach, E. A.; Gogotsi, Y. Modified MAX Phase Synthesis for Environmentally Stable and Highly Conductive Ti_3C_2 MXene. *ACS Nano* **2021**, *15* (4), 6420−6429.
(43) Facure, M. H. M.; Matthews, K.; Wang, R.; Lord, R. W.; Correa, D. S.; Gogotsi, Y. Pillaring Effect of Nanodiamonds and Expanded Voltage Window of $Ti_3C_2T_x$ Supercapacitors in $AlCl_3$ Electrolyte. *Energy Storage Mater.* **2023**, *61*, No. 102919.
(44) Facure, M. H. M.; Andre, R. S.; Mercante, L. A.; Correa, D. S. Colorimetric Detection of Antioxidants in Food Samples Using MnO_2/Graphene Quantum Dot Composites with Oxidase-like Activity. *ACS Appl. Nano Mater.* **2022**, *5* (10), 15211−15219.
(45) Jiang, B.; Duan, D.; Gao, L.; Zhou, M.; Fan, K.; Tang, Y.; Xi, J.; Bi, Y.; Tong, Z.; Gao, G. F.; Xie, N.; Tang, A.; Nie, G.; Liang, M.; Yan, X. Standardized Assays for Determining the Catalytic Activity and Kinetics of Peroxidase-like Nanozymes. *Nat. Protoc* **2018**, *13* (7), 1506−1520.
(46) Shi, W.; Wang, Q.; Long, Y.; Cheng, Z.; Chen, S.; Zheng, H.; Huang, Y. Carbon Nanodots as Peroxidase Mimetics and Their Applications to Glucose Detection. *Chem. Commun.* **2011**, *47* (23), 6695−6697.
(47) Shekhirev, M.; Shuck, C. E.; Sarycheva, A.; Gogotsi, Y. Characterization of MXenes at Every Step, from Their Precursors to Single Flakes and Assembled Films. *Prog. Mater. Sci.* **2021**, *120*, No. 100757.
(48) Li, Y.; Zhao, J.; Dan, Y.; Ma, D.; Zhao, Y.; Hou, S.; Lin, H.; Wang, Z. Low Temperature Aqueous Synthesis of Highly Dispersed Co_3O_4 Nanocubes and Their Electrocatalytic Activity Studies. *Chemical Engineering Journal* **2011**, *166* (1), 428−434.
(49) Konan, F. K.; N'cho, J. S.; Nkuissi, H. J. T.; Hartiti, B.; Boko, A. Influence of the Precursor Concentration on the Morphological and Structural Properties of Zinc Oxide (ZnO). *Mater. Chem. Phys.* **2019**, *229*, 330−333.
(50) Lipatov, A.; Alhabeb, M.; Lukatskaya, M. R.; Boson, A.; Gogotsi, Y.; Sinitskii, A. Effect of Synthesis on Quality, Electronic Properties and Environmental Stability of Individual Monolayer Ti_3C_2 MXene Flakes. *Adv. Electron Mater.* **2016**, *2* (12), No. 1600255.
(51) Liu, D.; Li, T.; Sun, W.; Zhou, W.; Zhang, G. Magnetic Ti_3C_2 MXene Nanomaterials for Doxorubicin Adsorption from Aqueous Solutions: Kinetic, Isotherms, and Thermodynamic Studies. *ACS Omega* **2022**, *7* (36), 31945−31953.
(52) Kiran, N. U.; Deore, A. B.; More, M. A.; Late, D. J.; Rout, C. S.; Mane, P.; Chakraborty, B.; Besra, L.; Chatterjee, S. Comparative Study of Cold Electron Emission from 2D $Ti_3C_2T_X$ MXene Nanosheets with Respect to Its Precursor Ti_3SiC_2 MAX Phase. *ACS Appl. Electron Mater.* **2022**, *4* (6), 2656−2666.
(53) Li, Y.; Zhou, X.; Wang, J.; Deng, Q.; Li, M.; Du, S.; Han, Y.-H.; Lee, J.; Huang, Q. Facile Preparation of in Situ Coated $Ti_3C_2T_x$/$Ni_{0.5}Zn_{0.5}Fe_2O_4$ Composites and Their Electromagnetic Performance. *RSC Adv.* **2017**, *7* (40), 24698−24708.
(54) Gadisa, B. T.; Kassahun, S. K.; Appiah-Ntiamoah, R.; Kim, H. Tuning the Charge Carrier Density and Exciton Pair Separation in Electrospun 1D ZnO-C Composite Nanofibers and Its Effect on Photodegradation of Emerging Contaminants. *J. Colloid Interface Sci.* **2020**, *570*, 251−263.
(55) Ali, Md. A.; Mondal, K.; Singh, C.; Dhar Malhotra, B.; Sharma, A. Anti-Epidermal Growth Factor Receptor Conjugated Mesoporous Zinc Oxide Nanofibers for Breast Cancer Diagnostics. *Nanoscale* **2015**, *7* (16), 7234−7245.
(56) Tammina, S. K.; Yang, D.; Li, X.; Koppala, S.; Yang, Y. High Photoluminescent Nitrogen and Zinc Doped Carbon Dots for Sensing Fe^{3+} Ions and Temperature. *Spectrochim Acta A Mol. Biomol Spectrosc* **2019**, *222*, No. 117141.
(57) Das, P.; Ganguly, S.; Bose, M.; Mondal, S.; Choudhary, S.; Gangopadhyay, S.; Das, A. K.; Banerjee, S.; Das, N. C. Zinc and Nitrogen Ornamented Bluish White Luminescent Carbon Dots for Engrossing Bacteriostatic Activity and Fenton Based Bio-Sensor. *Materials Science and Engineering: C* **2018**, *88*, 115−129.
(58) Tammina, S. K.; Wan, Y.; Li, Y.; Yang, Y. Synthesis of N, Zn-Doped Carbon Dots for the Detection of Fe^{3+} Ions and Bactericidal Activity against Escherichia Coli and Staphylococcus Aureus. *J. Photochem. Photobiol. B* **2020**, *202*, No. 111734.
(59) Huang, J.; Zhang, S.; Qin, Q.; Wang, Z.; Cai, G. Designing V_2O_5/MXene van Der Waals Heterostructure for Complementary Electrochromic Dual-Ion Capacitor. *Chemical Engineering Journal* **2023**, *476*, No. 146626.
(60) Zhang, J.; Kong, N.; Uzun, S.; Levitt, A.; Seyedin, S.; Lynch, P. A.; Qin, S.; Han, M.; Yang, W.; Liu, J.; Wang, X.; Gogotsi, Y.; Razal, J. M. Scalable Manufacturing of Free-Standing, Strong $Ti_3C_2T_x$ MXene Films with Outstanding Conductivity. *Adv. Mater.* **2020**, *32* (23), No. 2001093.
(61) Shuck, C. E.; Sarycheva, A.; Anayee, M.; Levitt, A.; Zhu, Y.; Uzun, S.; Balitskiy, V.; Zahorodna, V.; Gogotsi, O.; Gogotsi, Y.

Scalable Synthesis of $Ti_3C_2T_x$ MXene. *Adv. Eng. Mater.* **2020**, *22* (3), No. 1901241.
(62) Dillip, G. R.; Banerjee, A. N.; Anitha, V. C.; Deva Prasad Raju, B.; Joo, S. W.; Min, B. K. Oxygen Vacancy-Induced Structural, Optical, and Enhanced Supercapacitive Performance of Zinc Oxide Anchored Graphitic Carbon Nanofiber Hybrid Electrodes. *ACS Appl. Mater. Interfaces* **2016**, *8* (7), 5025−5039.
(63) Andre, R. S.; Campaner, K.; Facure, M. H. M.; Mercante, L. A.; Bogusz, S.; Correa, D. S. Nanocomposite-Based Chemiresistive Electronic Nose and Application in Coffee Analysis. *ACS Food Science & Technology* **2021**, *1*, 1464−1471.
(64) Li, X.; Ren, K.; Zhang, M.; Sang, W.; Sun, D.; Hu, T.; Ni, Z. Cobalt Functionalized MoS_2/Carbon Nanotubes Scaffold for Enzyme-Free Glucose Detection with Extremely Low Detection Limit. *Sens Actuators B Chem.* **2019**, *293*, 122−128.
(65) Hwang, H.; Byun, S.; Yuk, S.; Kim, S.; Song, S. H.; Lee, D. High-Rate Electrospun $Ti_3C_2T_x$ MXene/Carbon Nanofiber Electrodes for Flexible Supercapacitors. *Appl. Surf. Sci.* **2021**, *556* (March), No. 149710.
(66) He, J.; Yang, L.; Zhang, Y.; Li, R.; Wu, J.; Cao, Q.; Li, S.; Wu, X.; Duan, Y.; He, D.; Wang, W. Pd-Pt-Ru Nanozyme with Peroxidase-like Activity for the Detection of Total Antioxidant Capacity. *Analytical Methods* **2022**, *15* (1), 8−16.
(67) Lou, Z.; Zhao, S.; Wang, Q.; Wei, H. N-Doped Carbon as Peroxidase-Like Nanozymes for Total Antioxidant Capacity Assay. *Anal. Chem.* **2019**, *91* (23), 15267−15274.
(68) Moreno-Castilla, C.; Naranjo, Á.; Victoria López-Ramón, M.; Siles, E.; López-Peñalver, J. J.; de Almodóvar, J. M. R. Influence of the Hydrodynamic Size and ζ Potential of Manganese Ferrite Nanozymes as Peroxidase-Mimicking Catalysts at pH 4 in Different Buffers. *J. Catal.* **2022**, *414*, 179−185.
(69) Zhang, L.; Hai, X.; Xia, C.; Chen, X.-W.; Wang, J.-H. Growth of CuO Nanoneedles on Graphene Quantum Dots as Peroxidase Mimics for Sensitive Colorimetric Detection of Hydrogen Peroxide and Glucose. *Sens Actuators B Chem.* **2017**, *248*, 374−384.
(70) Cheng, N.; Li, J.-C.; Liu, D.; Lin, Y.; Du, D. Single-Atom Nanozyme Based on Nanoengineered Fe−N−C Catalyst with Superior Peroxidase-Like Activity for Ultrasensitive Bioassays. *Small* **2019**, *15* (48), No. 1901485.
(71) Liu, J.; Guo, X.; Huang, H.; Cui, R.; Wang, D.; Chen, Y.; Chai, Y.; Dong, J.; Sun, B.; Lian, Y. Enhanced Peroxidase-like Activity of Graphdiyne-Based Nanozymes by Fe and N Codoping for Colorimetric Determination of H_2O_2 and Ascorbic Acid. *ACS Appl. Nano Mater.* **2023**, *6* (23), 22142−22151.
(72) Liu, W.; Chu, L.; Zhang, C.; Ni, P.; Jiang, Y.; Wang, B.; Lu, Y.; Chen, C. Hemin-Assisted Synthesis of Peroxidase-like Fe-N-C Nanozymes for Detection of Ascorbic Acid-Generating Bio-Enzymes. *Chemical Engineering Journal* **2021**, *415*, No. 128876.
(73) Yin, D.; Cao, X.; Liu, X.; Yang, Z.; Liu, Z.; Wang, D.; Liu, Q.; Zhang, X.; Zhang, X. Rapid Colorimetric Sensing of Ascorbic Acid Based on the Excellent Peroxidase-like Activity of Pt Deposited on $ZnCo_2O_4$ Spheres. *New J. Chem.* **2020**, *44* (28), 12002−12008.
(74) Isho, R. D.; Sher Mohammad, N. M.; Omer, K. M. Enhancing Enzymatic Activity of Mn@Co_3O_4 Nanosheets as Mimetic Nanozyme for Colorimetric Assay of Ascorbic Acid. *Anal. Biochem.* **2022**, *654* (June), No. 114818.
(75) Hao, P.; Liu, Y.; Wang, L.; Zhu, X.; Liu, Q. Nanozyme Sensor Array Based on Porphyrin-Modified $CoMoO_4$ to Detect and Distinguish Biologically Important Thiols. *ACS Appl. Nano Mater.* **2023**, *6* (3), 1937−1947.
(76) Wang, T.; Feng, J.; Sun, H.; Liang, Y.; Du, T.; Dan, J.; Wang, J.; Zhang, W. CuBi Bimetallic Aerogel as Peroxidase-like Nanozyme for Total Antioxidant Capacity Colorimetric Detection. *Sens Actuators B Chem.* **2023**, *379*, No. 133249.
(77) Ma, C.-B.; Xu, Y.; Wu, L.; Wang, Q.; Zheng, J.-J.; Ren, G.; Wang, X.; Gao, X.; Zhou, M.; Wang, M.; Wei, H. Guided Synthesis of a Mo/Zn Dual Single-Atom Nanozyme with Synergistic Effect and Peroxidase-like Activity. *Angew. Chem., Int. Ed.* **2022**, *61* (25), No. e202116170.
(78) Gao, L.; Zhuang, J.; Nie, L.; Zhang, J.; Zhang, Y.; Gu, N.; Wang, T.; Feng, J.; Yang, D.; Perrett, S.; Yan, X. Intrinsic Peroxidase-like Activity of Ferromagnetic Nanoparticles. *Nat. Nanotechnol* **2007**, *2* (9), 577−583.
(79) Xiao, X.; Zhang, Z.; Nan, F.; Zhao, Y.; Wang, P.; He, F.; Wang, Y. Mesoporous $CuCo_2O_4$ Rods Modified Glassy Carbon Electrode as a Novel Non-Enzymatic Amperometric Electrochemical Sensors with High-Sensitive Ascorbic Acid Recognition. *J. Alloys Compd.* **2021**, *852*, No. 157045.
(80) Maseed, H.; Reddy Yenugu, V. M.; Devarakonda, S. S.; Petnikota, S.; Gajulapalli, M.; Srikanth, V. V. S. S. Peroxidase-like Fe_3O_4 Nanoparticle/Few-Layered Graphene Composite for Electrochemical Detection of Dopamine, Ascorbic Acid, and Uric Acid. *ACS Appl. Nano Mater.* **2023**, *6* (19), 18531−18538.
(81) Hasan, Md. M.; Reza, Md. A.; Haque, A. Detection and Quantification of Ascorbic Acid in Citrus Macroptera Fruit Pulp Juice by High Performance Liquid Chromatography. *Analytical Chemistry Letters* **2021**, *11* (2), 284−288.
(82) Bhaiyya, M.; Pattnaik, P. K.; Goel, S. Simultaneous Detection of Vitamin B12 and Vitamin C from Real Samples Using Miniaturized Laser-Induced Graphene Based Electrochemiluminescence Device with Closed Bipolar Electrode. *Sens Actuators A Phys.* **2021**, *331*, No. 112831.
(83) Ning, Y.; Sun, Y.; Yang, X.; Li, Y.; Han, A.; Wang, B.; Liu, J. Defect-Rich CoFe-Layered Double Hydroxides as Superior Peroxidase-like Nanozymes for the Detection of Ascorbic Acid. *ACS Appl. Mater. Interfaces* **2023**, *15* (22), 26263−26272.
(84) Yan, B.; Yang, Y.; Xie, Y.; Li, J.; Li, K. Fe Doping Enhances the Peroxidase-Like Activity of CuO for Ascorbic Acid Sensing. *Chemistry.* **2023**, *5*, 1302−1316.
(85) Yang, W.; Li, J.; Wang, M.; Sun, X.; Liu, Y.; Yang, J.; Ng, D. H. L. A Colorimetric Strategy for Ascorbic Acid Sensing Based on the Peroxidase-like Activity of Core-Shell Fe_3O_4/CoFe-LDH Hybrid. *Colloids Surf. B Biointerfaces* **2020**, *188*, No. 110742.
(86) He, J.; He, D.; Yang, L.; Wu, G.-L.; Tian, J.; Liu, Y.; Wang, W. Preparation of Urchin-like Pd-Pt-Ir Nanozymes and Their Application for the Detection of Ascorbic Acid and Hydrogen Peroxide. *Mater. Lett.* **2022**, *314*, No. 131851.

https://doi.org/10.1021/acsanm.4c00539
ACS Appl. Nano Mater. 2025, 8, 4291−4299